

Robust Electronic Structure of Manganite-Buffered Oxide Interfaces with Extreme Mobility Enhancement

Hang Li, Yulin Gan, Marius-Adrian Husanu, Rasmus Tindal Dahm, Dennis Valbjørn Christensen, Milan Radovic, Jirong Sun, Ming Shi, Baogen Shen, Nini Pryds*, and Yunzhong Chen*



Cite This: ACS Nano 2022, 16, 6437–6443



Read Online

ACCESS |

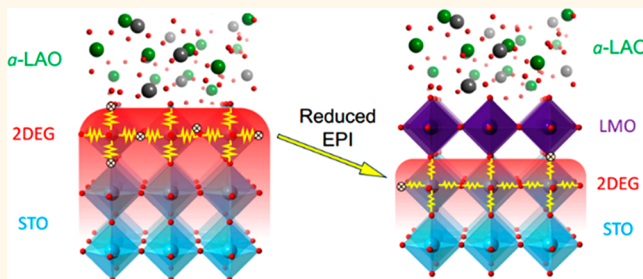
Metrics & More

Article Recommendations

Supporting Information

ABSTRACT: The electronic structure as well as the mechanism underlying the high-mobility two-dimensional electron gases (2DEGs) at complex oxide interfaces remain elusive. Herein, using soft X-ray angle-resolved photoemission spectroscopy (ARPES), we present the band dispersion of metallic states at buffered LaAlO₃/SrTiO₃ (LAO/STO) heterointerfaces where a single-unit-cell LaMnO₃ (LMO) spacer not only enhances the electron mobility but also renders the electronic structure robust toward X-ray radiation. By tracing the evolution of band dispersion, orbital occupation, and electron–phonon interaction of the interfacial 2DEG, we find unambiguous evidence that the insertion of the LMO buffer strongly suppresses both the formation of oxygen vacancies as well as the electron–phonon interaction on the STO side. The latter effect makes the buffered sample different from any other STO-based interfaces and may explain the maximum mobility enhancement achieved at buffered oxide interfaces.

KEYWORDS: oxide interfaces, high mobility 2DEG, electronic structure, electron–phonon interaction, resonant angle-resolved photoemission spectroscopy



INTRODUCTION

The two-dimensional electron gas (2DEG) formed at the interface between two oxide band insulators, LaAlO₃/SrTiO₃ (LAO/STO), in particular,¹ exhibits exotic physical properties such as superconductivity,^{2–6} magnetism,^{7–10} Rashba-type spin–orbit coupling,^{11,12} and the quantum Hall effect.^{13,14} However, the origin of the conduction as well as the role of as-grown defects such as oxygen vacancies (OVs) on the conduction have often been topics of hot debate. In addition to the polar discontinuity-induced electronic and ionic reconstructions,^{1,15–17} OVs resulting from vacuum annealing,^{16–19} light irradiation,^{20–24} or interfacial redox reaction^{25–27} could also generate electrons, giving a large or even dominating contribution to the conduction. Regardless of the exact origin of the conduction, for most 2DEG systems related to STO, bare STO surface, or STO-based interfaces, the itinerant charges occupy the conduction band of STO with lower energy, which consists of exclusively Ti t_{2g} (d_{xy} and d_{xz}/d_{yz}) orbitals (Figure 1a).^{28–31} The electrons of the d_{xy} orbitals, contributing to the most carrier concentration, are strongly confined near the surface/interface of STO, forming quasi-2D subbands (Figure 1a), known as the light band with low

effective mass. Meanwhile, the d_{xz}/d_{yz} orbitals construct heavy bands with large effective mass while their wave functions extend deep into the bulk STO resulting in quasi-3D character (Figure 1 a).³² As for the band character of each t_{2g} band, d_{xy} orbitals construct the circular electron pocket at the Fermi surface (FS), and the other two elliptical pockets are constructed by d_{xz} and d_{yz} orbitals, as revealed in Figure 1d. Compared with heavy d_{xz}/d_{yz} bands, the light d_{xy} band hosts larger bandwidth and smaller Fermi momenta (k_F) (Figure 1d).

Despite the intensive research, to date, one of the key challenges of STO 2DEGs is increasing the carrier mobility and revealing the underlying mechanism. The d_{xy} electrons, residing in closer proximity to the interface, have a smaller effective mass compared to the d_{xz}/d_{yz} ones, but their mobility

Received: January 18, 2022

Accepted: March 16, 2022

Published: March 21, 2022



ACS Publications

© 2022 American Chemical Society

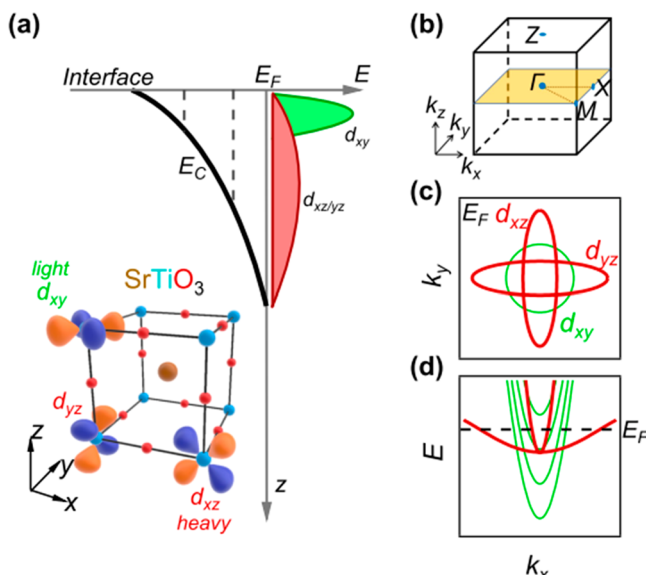


Figure 1. (a) Quantum-well states of 2DEG formed by wedgelike potential near the surface/interface of STO. Bold black curve shows the conduction band profile (E_C). The insert panel shows the unit cell and $d_{xy}/d_{xz}/d_{yz}$ orbitals of STO. The positive and negative lobes of the orbitals are shown in orange and blue, respectively. (b) 3D Brillouin zone (BZ) of STO-based systems. (c,d) Typical FS pattern and electronic structure of a STO 2DEG system, respectively.

is often lower probably due to a large defect concentration at the interface.³³ For most STO-based 2DEGs, the typical carrier mobility is around $1000 \text{ cm}^2 \text{ V}^{-1} \text{ s}^{-1}$ at low temperatures. This is expected to be further decreased under light irradiation in

high vacuum as significant oxygen-deficiency develops during light exposure.^{22,32–34} Notably, recent studies show that the carrier mobility can be significantly enhanced by deliberate surface or interface engineering.^{35–41} One significant example is the insertion of a single unit cell of epitaxial LaMnO₃ (LMO) at the interface between amorphous-LaAlO₃ and STO substrate (*a*-LAO/LMO/STO),³⁹ where an electron sink of Mn³⁺ in the perovskite structure was used to decrease the carrier density of 2DEG on the STO side through interfacial charge transfer.³⁹ The introduction of the manganite buffer layer decreases the carrier density by approximately 1 order of magnitude, whereas the carrier mobility is increased 10–100 times compared to the unbuffered *a*-LAO/STO.³⁹ It also leads to the observation of a clear quantum Hall effect at complex oxide interfaces.¹³ However, the electronic structure of these buffered oxide interfaces with enhanced carrier mobility remains to be determined. Identifying the electronic structure as well as the orbital configuration becomes even more interesting upon the recent finding that the high mobility 2DEG at $\gamma\text{-Al}_2\text{O}_3/\text{STO}$ (GAO/STO) interface shows an anomaly in orbital ordering as well as a weak electron–phonon interaction (EPI) strength of the carriers.^{42,43}

In this paper, we identify the electronic band structure of the buried oxide interfaces by soft X-ray angle-resolved photoemission spectroscopy (ARPES) for both bare and LMO-buffered *a*-LAO/STO. Besides a slight decrease in the k_F and carrier density as well as a strong suppression in the concentration of OVs,³⁹ the buffered interface exhibits two significant properties: (1) an unexpected irradiation-robust band structure, which reflects the detection of FS of intrinsic interface states, and (2) a significantly reduced EPI strength, which is absent in the nonbuffered^{42,43} as well as the diluted crystalline LAO/STO interfaces. The combined effect of the

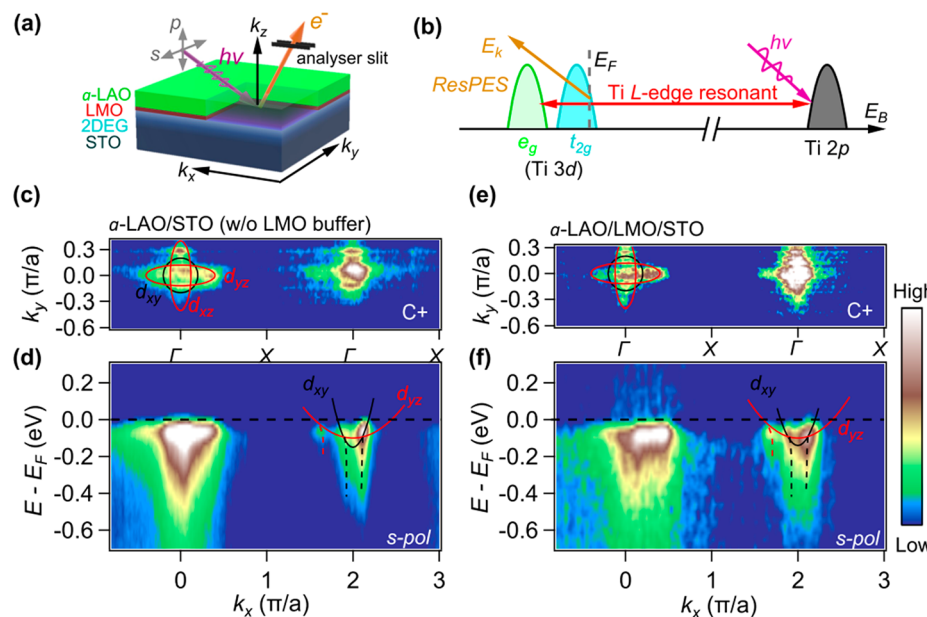


Figure 2. (a) Sketches of the modulation-doped *a*-LAO/LMO/STO with the experimental geometry for the ARPES measurement. The gray arrows represent the *s*- and *p*-polarization of X-rays. (b) Sketches of resonant photoemission process in STO-based 2DEG systems. (c,e) FS maps and band dispersions measured at C + polarization of *a*-LAO/STO and *a*-LAO/LMO/STO ($t = 1\mu\text{c}$) at E_F in $k_z = 0$ plane, respectively. The black circles and red ellipses indicate the FS of d_{xy} and d_{xz}/d_{yz} orbitals, respectively. (d,f) Electronic structures along k_z measured with *s*-polarization of *a*-LAO/STO and *a*-LAO/LMO/STO, respectively. Black and red curves mark the band structure of d_{xy} and d_{yz} orbitals, respectively. Black and red dashed curves mark the pronounced tail of polarons induced by EPI. All data are recorded at Ti *L*-edge resonant energy, which corresponds to the $k_z = 7 \times 2 \pi/a$ plane in the BZ of STO (Figure S1).

reduction in the carrier density, the suppression of defect concentration of OVs, as well as the decrease in the EPI strength on the STO side could account for the extreme mobility of the buffered oxide heterostructures.

RESULTS AND DISCUSSION

The interfacial 2DEG locates on the STO side in close proximity to the interface underneath the capping layer, which is generally thicker than 1.6 nm. To investigate the band structures of these heterostructures, we used soft X-ray ARPES, where the photoelectrons have an escape depth sufficiently large to probe buried interfaces,^{42–47} as illustrated in Figure 2a for *a*-LAO/LMO/STO.

First, we identified the FS maps and band dispersions for *a*-LAO/STO heterointerfaces with and without LMO buffer. The resonant photon energies are determined by $h\nu$ -dependent ARPES intensity map at E_F (see Figure S1). As revealed in Figure 2c,e, the experimental FS map consists of one circular electron pocket located at the center of Brillouin zone (BZ) and two other intersecting elliptical electron pockets aligned along the k_x and k_y directions (the two Γ –X directions in the BZ). This is a typical FS pattern of the STO-based 2DEG systems (Figure 1c).^{31,32,42,43}

The band dispersions of *a*-LAO/STO and *a*-LAO/LMO/STO ($t = 1$ uc) along the k_x direction were measured with linear *s*-polarized light (Figure 2a), which probe mostly the antisymmetric d_{xy} and d_{yz} orbitals, whereas the symmetric d_{xz} ones can be probed by the *p*-polarized light.^{44,45} As shown in Figure 2d,f, we can clearly identify the light d_{xy} band and heavy d_{yz} bands near the second Γ -point for *a*-LAO/STO and *a*-LAO/LMO/STO ($t = 1$ uc), respectively. Similar to most other STO-based systems, the Ti t_{2g} bands are reconstructed at the interface to form deep d_{xy} subbands and shallow $d_{xz/yz}$ bands (Figure 1d). This is due to the confined quantum well states with the bended band profiles near the surface region, which can be estimated by the binding energies of Ti 2p orbitals. However, our result (Figure S2) shows a similar value compared with pristine STO,⁴⁸ probably due to the limited energy resolutions. The pronounced intensity tail of these bands extending to higher binding energy is a sign of the strong polaronic coupling of charge carriers in these systems,^{42,43} which results in the discontinuity of band structures.

It has been found that STO-based 2DEG is often sensitive to the X-ray irradiation^{22,32,34,46} during ARPES measurements, where the photogenerated extra carriers could be used to tune the interface states, but it also makes the detection of the intrinsic electronic structure of interfacial 2DEGs challenging. Such an X-ray irradiation effect is demonstrated by the monotonous growth in the intensity of the 2DEG with respect to the X-ray exposure time as observed in *a*-LAO/STO (Figure 3a,c). On the contrary, we find that the intensity of the 2DEG in buffered sample shows a negligible increase during X-ray exposure (Figure 3b,c). The X-ray irradiation generated 2DEG is generally due to the formation of oxygen vacancies. We thus investigated the evolution of the in-gap states of OVs, which are located $E_B \sim 1.2$ eV below the Fermi energy level (E_F) (Figure S3). As shown in Figure 3d, the intensity of IGS for both buffered and unbuffered *a*-LAO/STO increases with respect to irradiation time. Notably, the intensity of the in-gap states increases at a rate much faster than that of the 2DEG for both samples, indicating that the photocreated OVs not only contribute to the extra mobile carriers but also localized

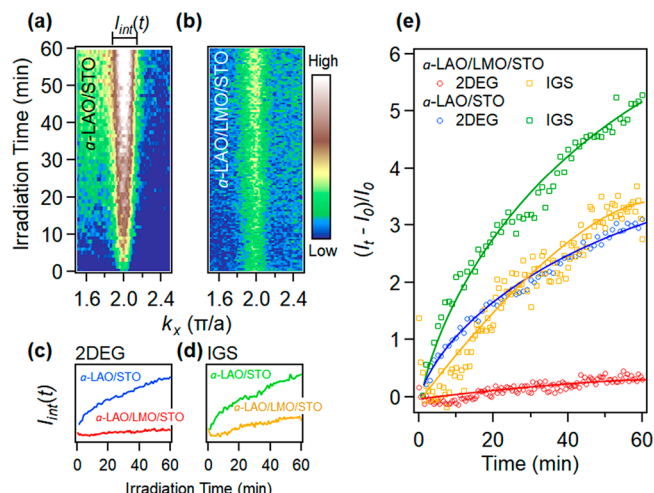


Figure 3. *k*-resolved intensity maps as a function of irradiation time at E_F of *a*-LAO/STO (a) and *a*-LAO/LMO/STO ($t = 1$ uc) (b), respectively. (c,d) Integrated intensities of 2DEG and OVs in-gap states (IGS) of *a*-LAO/STO and *a*-LAO/LMO/STO, respectively, as a function of irradiation time. (e) Time-dependent intensity change $[(I_t - I_0)/I_0]$ of 2DEG and OVs IGS for both *a*-LAO/STO and *a*-LAO/LMO/STO.

carriers. As far as *a*-LAO/LMO/STO is concerned, because of the nearly constant intensity of 2DEG with respect to X-ray irradiation, the difference in the intensity between the in-gap state of OVs and the 2DEG increases with respect to irradiation time although it has a slower rate compared to the unbuffered sample. This indicates two effects: first, the introduction of the LMO spacer suppresses the formation of OVs in the buffered sample; second, even though there are irradiation-induced in gap states in buffered samples, the photogenerated extra carriers are most likely transferred to the manganite buffer layer instead of 2DEG conduction layer. This is consistent with the electron sink role of LMO buffer layer. As a consequence, the LMO buffer layer renders the intrinsic electronic structure robust toward X-ray radiation.

Another feature of the buffered oxide interface is the strongly suppressed EPI. Besides electron–electron interactions, EPI is an important factor in STO affecting the charge transport and carrier mobility whereby the electrons drag behind a local perturbation of the crystal lattice as described by the concept of polarons.⁴⁴ Their signature in the experimental spectral function $A(\mathbf{k},\omega)$ is observed from the energy distribution curves (EDCs) as a peak-dip-hump structure, where the hump below the quasiparticle (QP) peak is formed by the EPI with the peak-to-hump distance reflecting the energy of the involved phonon modes. Figure 4c shows the EDCs of *a*-LAO/STO and *a*-LAO/LMO/STO, where the corresponding integration range is marked by the white box in Figure 4a,b for zoom-in band structures measured along k_x with *s*-polarized light. Both EDCs show clear QP peaks near E_F followed by an intensity tail at higher binding energy, consistent with previous observations in nonbuffered STO-based systems.^{42,44,45} The characteristic EPI-induced polaronic tail extends down to $E_b = -1$ eV. Notably, unlike stoichiometric crystalline LAO/STO⁴⁴ or GAO/STO,⁴² which exhibit clear satellite peaks for the LO₃ phonon mode, the hump lineshapes for these materials are structureless and extend over a wide energy range, suggesting that multiple phonon modes are involved in the EPI. The EPI strength is

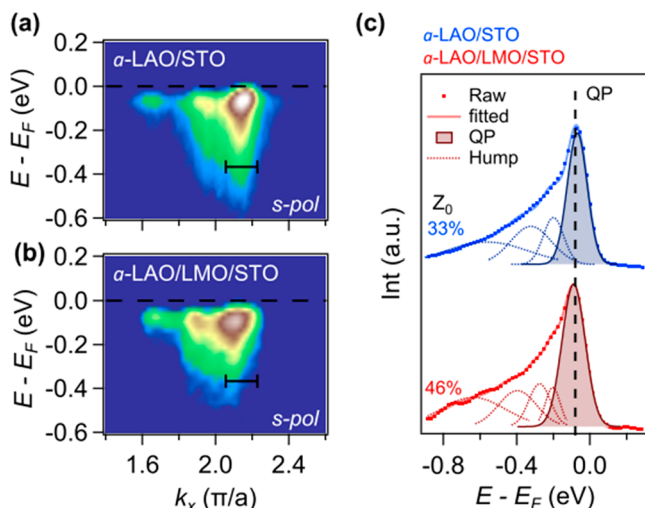


Figure 4. (a,b) Zoom-in band structures of $a\text{-LAO}/\text{STO}$ and modulation-doped $a\text{-LAO}/\text{LMO}/\text{STO}$ ($t = 1 \mu\text{m}$) measured along k_x with s -polarized light, respectively. (c) Integrated EDCs of d_{xy} orbitals (marked a and b). Red and blue dots show the raw integrated EDCs of $a\text{-LAO}/\text{LMO}/\text{STO}$ and $a\text{-LAO}/\text{STO}$, respectively. Filled dark red and blue curves show the fitted corresponding QP peaks. Dashed curves show the fitted hump peaks. Red and blue curves show the fitted EDCs combined by QP peaks and hump peaks.

related to the QP residual weight, Z_0 ,^{44,45} which is calculated as $Z_0 = I_{\text{QP}}/(I_{\text{QP}} + I_{\text{hump}})$, with I_{QP} and I_{hump} representing the integrated spectral weight of QP and residuals from EDCs, respectively. Larger Z_0 values identify heavier QP spectral weight thus smaller EPI. Our quantitative analyses show that Z_0 increases from 33% in $a\text{-LAO}/\text{STO}$ to 46% in $a\text{-LAO}/\text{LMO}/\text{STO}$ (Figure 4c). Since these two systems host a similar band structure and bandwidth (~ 80 meV in $a\text{-LAO}/\text{STO}$ and ~ 90 meV in $a\text{-LAO}/\text{LMO}/\text{STO}$, see the Supporting Information Figure S4), the increase in Z_0 suggests a significant decrease of EPI strength upon the introduction of the single unit cell LMO buffer, which can fundamentally enhance the carrier mobility as discussed below.⁴¹

In STO 2DEGs, the carrier mobility is limited by several crucial ingredients including defect concentration, strong EPI, and to a lesser extent, electron–electron correlations. The EPI will result in the polaronic nature of the interfacial charge carriers that increases their effective mass,⁴⁰ whereas defects at the interface will increase the impurity scattering of carriers. Both effects will decrease the carrier mobility. For the unbuffered $a\text{-LAO}/\text{STO}$, its concentration of OVs is high as expressed by the high intensity of in-gap states (Figure 3). The buffered sample shows much reduced in-gap states thus low OVs, which could explain partially the mobility enhancement. Notably, the Z_0 of the LMO-buffered sample increases to 46% in comparison to $\sim 33\%$ for $a\text{-LAO}/\text{STO}$. Previous studies on the temperature-dependent EPI effect of LAO/STO reveal that when Z_0 is increased from $\sim 30\%$ to $\sim 40\%$ the carrier mobility of 2DEG could be enhanced around 10 times.⁴⁴ It is noteworthy that a similar large Z_0 value of buffered sample is also obtained in GAO/STO,⁴² the carrier mobility of which can be up to $140000 \text{ cm}^2 \text{ V}^{-1} \text{ s}^{-1}$. Therefore, the nontrivial significant increase in Z_0 and, thus, the strong decrease in EPI of buffered oxide interfaces, on top of the suppression of the OVs, may be the main ingredient dominating the extreme mobility enhancement in buffered oxide interfaces. Addition-

ally, as the EPI is often associated with superconductivity in STO-based systems, the strong suppression of the EPI in $a\text{-LAO}/\text{LMO}/\text{STO}$ could well explain its absence of superconductivity.¹³

CONCLUSIONS

In summary, we have studied in detail the electronic structure by soft X-ray ARPES of buffered oxide interfaces with enhanced electron mobility. The ARPES results reveal a nontrivial feature of weakened EPI strength concomitant with decreased formation of oxygen vacancies. The combination of these effects could explain the mobility enhancement and provide crucial insights in boosting the carrier mobility of engineered oxide heterostructures as well as the design of quantum oxide devices.

METHODS

Sample Fabrication. All heterostructures, $a\text{-LAO}$ ($\sim 1.6 \text{ nm}$)/LMO/STO with different thicknesses of LMO buffer layer ($t = 0, 1$ and $2 \mu\text{m}$) were grown on TiO_2 -terminated STO substrates by pulse laser deposition (PLD) in an O_2 atmosphere of 10^{-4} mbar . A KrF pulse laser (248 nm in wavelength, 1 Hz repetition frequency, 4.0 J/cm^2 laser fluence) was adopted. For buffered/unbuffered $a\text{-LAO}/\text{STO}$, amorphous LAO deposited at room temperature under 10^{-4} mbar with single crystalline LAO as target. For the buffer layer, sintered LMO ceramics were used as targets and the growth temperature of LMO was fixed at 600°C . After the epitaxial growth of monolayer LMO buffer layer, the sample was cooled under the deposition pressure at a nominal rate of $15^\circ\text{C}/\text{min}$ to room temperature (below 30°C , in 5–6 h) before the subsequent $a\text{-LAO}$ film deposition *in situ*.

Angle-Resolved Photoemission Spectroscopy (ARPES). The soft-X-ray ARPES measurements were performed at the ADRESS beamline^{49,50} of the Swiss Light Source at Paul Scherrer Institute, Switzerland. The ARPES maps were recorded with a PHOIBOS-150 analyzer at an energy resolution of 60 meV and angular resolution of 0.1° . The samples were transferred *ex situ* and measured in the ARPES setup without annealing. All measurements are acquired at 12 K in a base pressure of better than $5 \times 10^{-11} \text{ Torr}$.

ASSOCIATED CONTENT

Supporting Information

The Supporting Information is available free of charge at <https://pubs.acs.org/doi/10.1021/acsnano.2c00609>.

Additional data, including summary of EPI strength (Z_0), concentration of the oxygen vacancies (n_{OV}), Fermi momenta (k_F) of d_{xy} and d_{yz} bands, carrier density (n_s), and carrier mobility (μ) of the studied samples; photon-energy-dependent result; XPS of $\text{Ti } 2p$ orbitals of $a\text{-LAO}/\text{STO}$ and $a\text{-LAO}/\text{LMO}/\text{STO}$; irradiation-dependent OV-states in $a\text{-LAO}/\text{LMO}/\text{STO}$ and $a\text{-LAO}/\text{STO}$; extraction of k_F ; ARPES result of $a\text{-LAO}/\text{LMO}/\text{STO}$ with 2 μm LMO buffer layer (PDF)

AUTHOR INFORMATION

Corresponding Authors

Yunzhong Chen – Beijing National Laboratory for Condensed Matter Physics and Institute of Physics, Chinese Academy of Sciences, 100190 Beijing, China; orcid.org/0000-0001-8368-5823; Email: yzchen@iphy.ac.cn

Nini Pryds – Department of Energy Conversion and Storage, Technical University of Denmark, 2800 Kgs. Lyngby, Denmark; orcid.org/0000-0002-5718-7924; Email: nipr@dtu.dk

Authors

Hang Li — Department of Energy Conversion and Storage, Technical University of Denmark, 2800 Kgs. Lyngby, Denmark; Swiss Light Source, Paul Scherrer Institute, 5232 Villigen, PSI, Switzerland

Yulin Gan — Beijing National Laboratory for Condensed Matter Physics and Institute of Physics, Chinese Academy of Sciences, 100190 Beijing, China

Marius-Adrian Husanu — National Institute of Materials Physics, 077125 Magurele, Romania; orcid.org/0000-0003-4510-6653

Rasmus Tindal Dahm — Department of Energy Conversion and Storage, Technical University of Denmark, 2800 Kgs. Lyngby, Denmark

Dennis Valbjørn Christensen — Department of Energy Conversion and Storage, Technical University of Denmark, 2800 Kgs. Lyngby, Denmark; orcid.org/0000-0003-0048-7595

Milan Radovic — Swiss Light Source, Paul Scherrer Institute, 5232 Villigen, PSI, Switzerland

Jirong Sun — Beijing National Laboratory for Condensed Matter Physics and Institute of Physics, Chinese Academy of Sciences, 100190 Beijing, China

Ming Shi — Swiss Light Source, Paul Scherrer Institute, 5232 Villigen, PSI, Switzerland

Baogen Shen — Beijing National Laboratory for Condensed Matter Physics and Institute of Physics, Chinese Academy of Sciences, 100190 Beijing, China

Complete contact information is available at:

<https://pubs.acs.org/10.1021/acsnano.2c00609>

Author Contributions

The manuscript was written through contributions of all authors. All authors have given approval to the final version of the manuscript. Y.Z.C. designed the concept and experiments with N.P.; H.L., Y.L.G., M.A.H., and R.T.D. performed the ARPES experiment; Y.L.G. and Y.Z.C. fabricated the samples and performed their transport characterization; H.L. and M.A.H. processed the ARPES data. All authors discussed the results and interpretations and wrote the manuscript.

Notes

The authors declare no competing financial interest.

ACKNOWLEDGMENTS

The authors thank V. N. Strocov for supporting the ARPES experiments and valuable advice at all stages of the work and T. Schmitt for supporting the beamline operation. B.G.S., J.R.S., and Y.Z.C. were supported by the Science Center of the National Science Foundation of China (52088101) and the National Key Research and Development Program of China (2021YFA1400300). Y.Z.C. also acknowledges support from the Independent Research Fund Denmark (Grant No. 9041-00034B). M.A.H. was supported by a grant from the Ministry of Research, Innovation and Digitization, CNCS/CCCDI-UEFISCDI, Project No. PCE 96, within PNCDI III. N.P. and D.V.C. acknowledge funding from the Villum Fonden (00027993) and Independent Research Fund Denmark (Grant No. 00069B).

REFERENCES

- (1) Ohtomo, A.; Hwang, H. Y. A High-Mobility Electron Gas at the LaAlO₃/SrTiO₃ Heterointerface. *Nature* **2004**, *427*, 423–426.

(2) Reyren, N.; Thiel, S.; Caviglia, A. D.; Fitting Kourkoutis, L.; Hammerl, G.; Richter, C.; Schneider, C. W.; Kopp, T.; Ruetschi, A.-S.; Jaccard, D.; Gabay, M.; Muller, D. A.; Triscone, J.-M.; Mannhart, J. Superconducting Interfaces Between Insulating Oxides. *Science* **2007**, *317*, 1196–1199.

(3) Caviglia, A. D.; Gariglio, S.; Reyren, N.; Jaccard, D.; Schneider, T.; Gabay, M.; Thiel, S.; Hammerl, G.; Mannhart, J.; Triscone, J. M. Electric Field Control of the LaAlO₃/SrTiO₃ Interface Ground State. *Nature* **2008**, *456*, 624–627.

(4) Joshua, A.; Pecker, S.; Ruhman, J.; Altman, E.; Ilani, S. A Universal Critical Density Underlying the Physics of Electrons at the LaAlO₃/SrTiO₃ Interface. *Nat. Commun.* **2012**, *3*, 1129.

(5) Prawiroatmodjo, G. E. D. K.; Trier, F.; Christensen, D. V.; Chen, Y.; Pryds, N.; Jespersen, T. S. Evidence of Weak Superconductivity at the Room-Temperature Grown LaAlO₃/SrTiO₃ Interface. *Phys. Rev. B* **2016**, *93*, 184504.

(6) Herranz, G.; Singh, G.; Bergeal, N.; Jouan, A.; Lesueur, J.; Gazquez, J.; Varela, M.; Scigaj, M.; Dix, N.; Sanchez, F.; Fontcuberta, J. Engineering Two-Dimensional Superconductivity and Rashba Spin–Orbit Coupling in LaAlO₃/SrTiO₃ Quantum Wells by Selective Orbital Occupancy. *Nat. Commun.* **2015**, *6*, 6028.

(7) Brinkman, A.; Huijben, M.; Van Zalk, M.; Huijben, J.; Zeitler, U.; Maan, J. C.; Van der Wiel, W. G.; Rijnders, G.; Blank, D. H. A.; Hilgenkamp, H. Magnetic Effects at the Interface Between Non-Magnetic Oxides. *Nat. Mater.* **2007**, *6*, 493–496.

(8) Kalisky, B.; Bert, J. A.; Klopfer, B. B.; Bell, C.; Sato, H. K.; Hosoda, M.; Hikita, Y.; Hwang, H. Y.; Moler, K. A. Critical Thickness for Ferromagnetism in LaAlO₃/SrTiO₃ Heterostructures. *Nat. Commun.* **2012**, *3*, 922.

(9) Bi, F.; Huang, M.; Ryu, S.; Lee, H.; Bark, C. W.; Eom, C. B.; Irvin, P.; Levy, J. Room-Temperature Electronically-Controlled Ferromagnetism at the LaAlO₃/SrTiO₃ Interface. *Nat. Commun.* **2014**, *5*, 5019.

(10) Christensen, D. V.; Frenkel, Y.; Chen, Y. Z.; Xie, Y. W.; Chen, Z. Y.; Hikita, Y.; Smith, A.; Klein, L.; Hwang, H. Y.; Pryds, N.; Kalisky, B. Strain-Tunable Magnetism at Oxide Domain Walls. *Nat. Phys.* **2019**, *15*, 269–274.

(11) Caviglia, A. D.; Gabay, M.; Gariglio, S.; Reyren, N.; Cancellieri, C.; Triscone, J.-M. Tunable Rashba Spin-Orbit Interaction at Oxide Interfaces. *Phys. Rev. Lett.* **2010**, *104*, 126803.

(12) Gan, Y.; Zhang, Y.; Christensen, D. V.; Pryds, N.; Chen, Y. Z. Gate-Tunable Rashba Spin-Orbit Coupling and Spin Polarization at Diluted Oxide Interfaces. *Phys. Rev. B* **2019**, *100*, 125134.

(13) Trier, F.; Prawiroatmodjo, G. E.D.K.; Zhong, Z.; Christensen, D. V.; Soosten, M.; Bhowmik, A.; Lastra, J. M. G.; Chen, Y.; Jespersen, T. S.; Pryds, N. Quantization of Hall Resistance at the Metallic Interface between an Oxide Insulator and SrTiO₃. *Phys. Rev. Lett.* **2016**, *117*, 096804.

(14) Matsubara, Y.; Takahashi, K. S.; Bahramy, M. S.; Kozuka, Y.; Maryenko, D.; Falson, J.; Tsukazaki, A.; Tokura, Y.; Kawasaki, M. Observation of the Quantum Hall Effect in δ -Doped SrTiO₃. *Nat. Commun.* **2016**, *7*, 11631.

(15) Nakagawa, N.; Hwang, H. Y.; Muller, D. A. Why Some Interfaces Cannot Be Sharp. *Nat. Mater.* **2006**, *5*, 204–209.

(16) Jang, H. W.; Felker, D. A.; Bark, C. W.; Wang, Y.; Niranjan, M. K.; Nelson, C. T.; Zhang, Y.; Su, D.; Folkman, C. M.; Baek, S. H.; Lee, S.; Janicka, K.; Zhu, Y.; Pan, X. Q.; Fong, D. D.; Tsymbal, E. Y.; Rzchowski, M. S.; Eom, C. B. Metallic and Insulating Oxide Interfaces Controlled by Electronic Correlations. *Science* **2011**, *331*, 886–889.

(17) Rose, M. A.; Šmid, B.; Vorokhta, M.; Slipukhina, I.; Andrä, M.; Bluhm, H.; Duchoň, T.; Ležaić, M.; Chambers, S. A.; Dittmann, R.; Mueller, D. N.; Gunkel, F. Identifying Ionic and Electronic Charge Transfer at Oxide Heterointerfaces. *Adv. Mater.* **2021**, *33*, 2004132.

(18) Thiel, S.; Hammerl, G.; Schmehl, A.; Schneider, C. W.; Mannhart, J. Tunable Quasi-Two-Dimensional Electron Gases in Oxide Heterostructures. *Science* **2006**, *313*, 1942–1945.

(19) Kalabukhov, A.; Gunnarsson, R.; Börjesson, J.; Olsson, E.; Claeson, T.; Winkler, D. Effect of Oxygen Vacancies in the SrTiO₃

- Substrate on the Electrical Properties of the LaAlO₃/SrTiO₃ Interface. *Phys. Rev. B* **2007**, *75*, No. 121404(R).
- (20) Gabel, J.; Zapf, M.; Scheiderer, P.; Schütz, P.; Dudy, L.; Stübinger, M.; Schlueter, C.; Lee, T. L.; Sing, M.; Claessen, R. Disentangling Specific Versus Generic Doping Mechanisms in Oxide Heterointerfaces. *Phys. Rev. B* **2017**, *95*, 195109.
- (21) Chikina, A.; Caputo, M.; Naamneh, M.; Christensen, D. V.; Schmitt, T.; Radovic, M.; Strocov, V. N. X-Ray Writing of Metallic Conductivity and Oxygen Vacancies at Silicon/SrTiO₃ Interfaces. *Adv. Funct. Mater.* **2019**, *29*, 1900645.
- (22) Strocov, V. N.; Chikina, A.; Caputo, M.; Husanu, M. A.; Bisti, F.; Bracher, D.; Schmitt, T.; Granozio, F. M.; Vaz, C. A. F.; Lechermann, F. Electronic Phase Separation at LaAlO₃/SrTiO₃ Interfaces Tunable by Oxygen Deficiency. *Phys. Rev. Mater.* **2019**, *3*, 106001.
- (23) Walker, S. M.; Bruno, F. Y.; Wang, Z.; Torre, A.; Riccò, S.; Tamai, A.; Kim, T. K.; Hoesch, M.; Shi, M.; Bahramy, M. S.; King, P. D. C.; Baumberger, F. Carrier-Density Control of the SrTiO₃ (001) Surface 2D Electron Gas Studied by ARPES. *Adv. Mater.* **2015**, *27*, 3894–3899.
- (24) Schütz, P.; Christensen, D. V.; Borisov, V.; Pfaff, F.; Scheiderer, P.; Dudy, L.; Zapf, M.; Gabel, J.; Chen, Y. Z.; Pryds, N.; Rogalev, V. A.; Strocov, V. N.; Lee, T. L.; Jeschke, H. O.; Valentí, R.; Sing, M.; Claessen, R. Microscopic Origin of the Mobility Enhancement at A Spinel/Perovskite Oxide Heterointerface Revealed by Photoemission Spectroscopy. *Phys. Rev. B* **2017**, *96*, 161409.
- (25) Chen, Y. Z.; Pryds, N.; Kleibeuker, J. E.; Sun, J. R.; Stamate, E.; Koster, G.; Shen, B. G.; Rijnders, G.; Linderoth, S. Metallic and Insulating Interfaces of Amorphous SrTiO₃-Based Oxide Heterostructures. *Nano Lett.* **2011**, *11*, 3774–3778.
- (26) Christensen, D. V.; Trier, F.; Soosten, M.; Prawiroatmodjo, G. E. D. K.; Jespersen, T. S.; Chen, Y. Z.; Pryds, N. Controlling Interfacial States in Amorphous/Crystalline LaAlO₃/SrTiO₃ Heterostructures by Electric Fields. *Appl. Phys. Lett.* **2013**, *102*, 021602.
- (27) Chen, Y. Z.; Pryds, N.; Sun, J. R.; Shen, B. G.; Linderoth, S. High-Mobility Two-Dimensional Electron Gases at Oxide Interfaces: Origins and Opportunities. *Chin. Phys. B* **2013**, *22*, 116803.
- (28) Gabay, M.; Triscone, J. M. Oxide Heterostructures: Hund Rules with a Twist. *Nat. Phys.* **2013**, *9*, 610–611.
- (29) Delugas, P.; Filippetti, A.; Fiorentini, V.; Bilc, D. I.; Fontaine, D.; Ghosez, P. Spontaneous 2-Dimensional Carrier Confinement at the n-Type SrTiO₃/LaAlO₃ Interface. *Phys. Rev. Lett.* **2011**, *106*, 166807.
- (30) Son, W. J.; Cho, E.; Lee, B.; Lee, J.; Han, S. Density and Spatial Distribution of Charge Carriers in the Intrinsic n-Type LaAlO₃-SrTiO₃ Interface. *Phys. Rev. B* **2009**, *79*, 245411.
- (31) Berner, G.; Sing, M.; Fujiwara, H.; Yasui, A.; Saitoh, Y.; Yamasaki, A.; Nishitani, Y.; Sekiyama, A.; Pavlenko, N.; Kopp, T.; Richter, C.; Mannhart, J.; Suga, S.; Claessen, R. Direct k-Space Mapping of the Electronic Structure in an Oxide–Oxide Interface. *Phys. Rev. Lett.* **2013**, *110*, 247601.
- (32) Plumb, N. C.; Salluzzo, M.; Razzoli, E.; Måansson, M.; Falub, M.; Krempasky, J.; Matt, C. E.; Chang, J.; Schulte, M.; Braun, J.; Ebert, H.; Minár, J.; Delley, B.; Zhou, K. J.; Schmitt, T.; Shi, M.; Mesot, J.; Patthey, L.; Radović, M. Mixed Dimensionality of Confined Conducting Electrons in the Surface Region of SrTiO₃. *Phys. Rev. Lett.* **2014**, *113*, 086801.
- (33) Santander-Syro, A. F.; Copie, O.; Kondo, T.; Fortuna, F.; Pailhès, S.; Weht, R.; Qiu, X. G.; Bertran, F.; Nicolaou, A.; Taleb-Ibrahimi, A.; Fèvre, P.; Herranz, G.; Bibes, M.; Reyren, N.; Apertet, Y.; Lecoeur, P.; Barthélémy, A.; Rozenberg, M. J. *Nature* **2011**, *469*, 189–193.
- (34) Meevasana, W.; King, P. D. C.; He, R. H.; Mo, S. K.; Hashimoto, M.; Tamai, A.; Songsiriritthigul, P.; Baumberger, F.; Shen, Z. X. Creation and Control of a Two-Dimensional Electron Liquid at the Bare SrTiO₃ Surface. *Nat. Mater.* **2011**, *10*, 114–118.
- (35) Huijben, M.; Koster, G.; Kruize, M. K.; Wenderich, S.; Verbeeck, J.; Bals, S.; Slooten, E.; Shi, B.; Molegraaf, H. J. A.; Kleibeuker, J. E.; van Aert, S.; Goedkoop, J. B.; Brinkman, A.; Blank, D. H. A.; Golden, M. S.; van Tendeloo, G.; Hilgenkamp, H.; Rijnders, G. Defect Engineering in Oxide Heterostructures by Enhanced Oxygen Surface Exchange. *Adv. Funct. Mater.* **2013**, *23*, 5240–5248.
- (36) Xie, Y. W.; Bell, C.; Hikita, Y.; Harashima, S.; Hwang, H. Y. Enhancing Electron Mobility at the LaAlO₃/SrTiO₃ Interface by Surface Control. *Adv. Mater.* **2013**, *25*, 4735–4738.
- (37) Chen, Y. Z.; Bovet, N.; Trier, F.; Christensen, D. V.; Qu, F. M.; Andersen, N. H.; Kasama, T.; Zhang, W.; Giraud, R.; Dufouleur, J.; Jespersen, T. S.; Sun, J. R.; Smith, A.; Nygård, J.; Lu, L.; Büchner, B.; Shen, B. G.; Linderoth, S.; Pryds, N. A High-Mobility Two-Dimensional Electron Gas at the Spinel/Perovskite Interface of γ -Al₂O₃/SrTiO₃. *Nat. Commun.* **2013**, *4*, 1371.
- (38) Chen, Y. Z.; Bovet, N.; Kasama, T.; Gao, W. W.; Yazdi, S.; Ma, C.; Pryds, N.; Linderoth, S. Room Temperature Formation of High-Mobility Two-Dimensional Electron Gases at Crystalline Complex Oxide Interfaces. *Adv. Mater.* **2014**, *26*, 1462–1467.
- (39) Chen, Y. Z.; Trier, F.; Wijnands, T.; Green, R. J.; Gauquelin, N.; Egoavil, R.; Christensen, D. V.; Koster, G.; Huijben, M.; Bovet, N.; Macke, S.; He, F.; Sutarto, R.; Andersen, N. H.; Sulpizio, J. A.; Honig, M.; Prawiroatmodjo, G. E. D. K.; Jespersen, T. S.; Linderoth, S.; Ilani, S.; Verbeeck, J.; Van Tendeloo, G.; Rijnders, G.; Sawatzky, G. A.; Pryds, N. Extreme Mobility Enhancement of Two-Dimensional Electron Gases at Oxide Interfaces by Charge-Transfer-Induced Modulation Doping. *Nat. Mater.* **2015**, *14*, 801–806.
- (40) Gan, Y. L.; Christensen, D. V.; Zhang, Y.; Zhang, H.; Krishnan, D.; Zhong, Z.; Niu, W.; Carrad, D. J.; Norrman, K.; Soosten, M.; Jespersen, T. S.; Shen, B. G.; Gauquelin, N.; Verbeeck, J.; Sun, J. R.; Pryds, N.; Chen, Y. Z. Diluted Oxide Interfaces with Tunable Ground States. *Adv. Mater.* **2019**, *31*, 1805970.
- (41) Chen, Y. Z.; Green, R. J.; Sutarto, R.; He, F.; Linderoth, S.; Sawatzky, G. A.; Pryds, N. Tuning the Two-Dimensional Electron Liquid at Oxide Interfaces by Buffer-Layer-Engineered Redox Reactions. *Nano Lett.* **2017**, *17*, 7062–7066.
- (42) Chikina, A.; Christensen, D. V.; Borisov, V.; Husanu, M. A.; Chen, Y. Z.; Wang, X. Q.; Schmitt, T.; Radovic, M.; Nagaosa, N.; Mishchenko, A. S.; Valentí, R.; Pryds, N.; Strocov, V. N. Band-Order Anomaly at the γ -Al₂O₃/SrTiO₃ Interface Drives the Electron-Mobility Boost. *ACS Nano* **2021**, *15*, 4347–4356.
- (43) Cao, Y. W.; Liu, X. R.; Shafer, P.; Middey, S.; Meyers, D.; Kareev, M.; Zhong, Z. C.; Kim, J. W.; Ryan, P. J.; Arenholz, E.; Chakhalian, J. Anomalous Orbital Structure in a Spinel–Perovskite Interface. *npj. quantum materials* **2016**, *1*, 16009.
- (44) Cancellieri, C.; Mishchenko, A. S.; Aschauer, U.; Filippetti, A.; Faber, C.; Barisić, O. S.; Rogalev, V. A.; Schmitt, T.; Nagaosa, N.; Strocov, V. N. Polaronic Metal State at the LaAlO₃/SrTiO₃ Interface. *Nat. Commun.* **2016**, *7*, 10386.
- (45) Strocov, V. N.; Cancellieri, C.; Mishchenko, A. S. Electrons and Polarons at Oxide Interfaces Explored by Soft-X-Ray ARPES. *Spectroscopy of Complex Oxide Interfaces*, Springer **2018**, 266, 107–151.
- (46) Strocov, V. N. Photoemission Response of 2D Electron States. *J. Electron Spectrosc. Relat. Phenom.* **2018**, *229*, 100–107.
- (47) Cancellieri, C.; Reinle-Schmitt, M. L.; Kobayashi, M.; Strocov, V. N.; Willmott, P. R.; Fontaine, D.; Ghosez, P.; Filippetti, A.; Delugas, P.; Fiorentini, V. Doping-Dependent Band Structure of LaAlO₃/SrTiO₃ Interfaces by Soft X-Ray Polarization-Controlled Resonant Angle-Resolved Photoemission. *Phys. Rev. B* **2014**, *89*, No. 121412(R).
- (48) Chambers, S. A.; Sushko, P. V. Influence of Crystalline Order and Defects on the Absolute Work Functions and Electron Affinities of TiO₂- and SrO-Terminated n-SrTiO₃(001). *Phys. Rev. Mater.* **2019**, *3*, 125803.
- (49) Strocov, V. N.; Wang, X.; Shi, M.; Kobayashi, M.; Krempasky, J.; Hess, C.; Schmitt, T.; Patthey, L. Soft-X-ray ARPES Facility at the ADRESS Beamline of the SLS: Concepts, Technical Realisation and Scientific Applications. *J. Synchrotron Rad.* **2014**, *21*, 32–44.
- (50) Strocov, V. N.; Schmitt, T.; Flechsig, U.; Schmidt, T.; Imhof, A.; Chen, Q.; Raabe, J.; Betemps, R.; Zimoch, D.; Krempasky, J.; Wang, X.; Grioni, M.; Piazzalunga, A.; Patthey, L. High-Resolution

Soft X-ray Beamline ADRESS at the Swiss Light Source for Resonant Inelastic X-ray Scattering and Angle-Resolved Photoelectron Spectroscopies. *J. Synchrotron Rad.* **2010**, *17*, 631–643.

□ Recommended by ACS

Emergence of Quasi Two-Dimensional Electronic States at the Interface of LSMO/STO via Lattice Mismatch-Induced Strains

Satya Prakash Pati, Tomoyasu Taniyama, *et al.*

AUGUST 17, 2022

ACS APPLIED ELECTRONIC MATERIALS

READ ▶

Current Mapping of Amorphous LaAlO₃/SrTiO₃ near the Metal–Insulator Transition

Anders V. Bjørlig, Beena Kalisky, *et al.*

JULY 01, 2022

ACS APPLIED ELECTRONIC MATERIALS

READ ▶

Surface Atomic Decoration of a Manganite to a Modular Oxygen Evolution Reaction

Ji Qi, Weiming Lü, *et al.*

DECEMBER 16, 2021

ACS APPLIED MATERIALS & INTERFACES

READ ▶

Atomic-Scale Tuning of the Charge Distribution by Strain Engineering in Oxide Heterostructures

Yu-Mi Wu, Peter A. van Aken, *et al.*

SEPTEMBER 30, 2021

ACS NANO

READ ▶

[Get More Suggestions >](#)
